Colloids and Surfaces A: Physicochemical and Engineering Aspects 726 (2025) 138110

Contents lists available at ScienceDirect

Colloids and Surfaces A: Physicochemical and Engineering Aspects

journal homepage: www.elsevier.com/locate/colsurfa

Novel insights into mechanical behavior of hydrogen-functionalized TPG and NTPG nanosheets via molecular dynamics simulations

Amirhossein Nikparsa [a], Reza Ansari [a,c,**], Mohsen Eghbalian [a], Saeid Sahmani [b,c,*], Eligiusz Postek [b]

[a] Faculty of Mechanical Engineering, University of Guilan, Rasht 3756, Iran
[b] Institute of Fundamental Technological Research, Polish Academy of Sciences, Pawińskiego 5B, Warsaw 02-106, Poland
[c] Department of Civil Engineering, School of Science and Technology, The University of Georgia, Tbilisi 0171, Georgia

GRAPHICAL ABSTRACT

Stress-Strain curve for NTPG nanosheet applying H- functionalization along with x-axis and y-axis

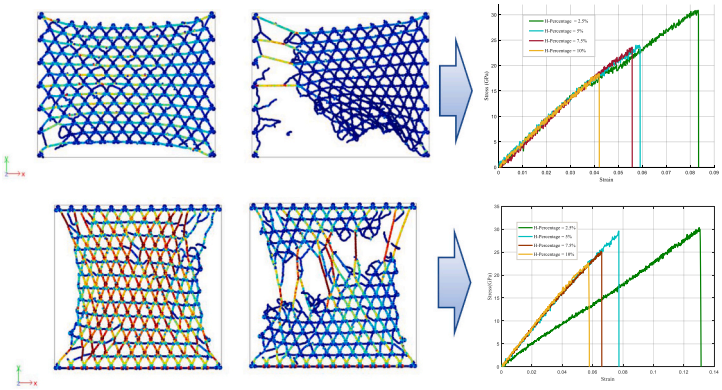

ARTICLE INFO

Keywords:
Triphenylene graphdiyne
Nitrogen-doped TPG
Hydrogen functionalization
Molecular dynamics simulation
Mechanical properties

ABSTRACT

Triphenylene-based graphdiyne (TPG) and nitrogen-doped TPG (NTPG) are recently developed two-dimensional nanomaterials with promising mechanical and electronic potential. The current study presents the first exploration of the hydrogen-functionalized TPG and NTPG nanosheets subjected to a uniaxial tensile loading condition using molecular dynamics simulations. The developed computational approach introduces a novel random functionalization scheme to improve the attributed structural stability. The Tersoff potential is employed to model the intra-layer interactions within the TPG. On the other hand, the interactions at the site of functionalization are described by the Dreiding force field for C and H atoms, supplemented by the Lennard-Jones (LJ) potential. The minimization process is applied via the conjugate-gradient technique, and following that, the system undergoes a canonical ensemble (NVT) simulation at 300 K with a timestep of 0.001 ps. In this step, the Nose–Hoover thermostat algorithm controlled the fluctuation of thermodynamic parameters, and the structure surpassed a stable status. The achieved numerical results demonstrate that hydrogen coverage significant

* Corresponding author at: Institute of Fundamental Technological Research, Polish Academy of Sciences, Pawinskiego 5B, Warsaw 02-106, Poland.
** Corresponding author at: Faculty of Mechanical Engineering, University of Guilan, Rasht 3756, Iran.
E-mail addresses: r_ansari@guilan.ac.ir (R. Ansari), ssahmani@ippt.pan.pl (S. Sahmani).

https://doi.org/10.1016/j.colsurfa.2025.138110
Received 5 July 2025; Received in revised form 7 August 2025; Accepted 20 August 2025
Available online 20 August 2025

influences on the mechanical behavior, including failure stress and strain, Young's modulus and toughness of TPG as well as NTPG nanosheets. For the both of nanosheets, increasing the hydrogen functionalization from 2.5 % to 10 % results in a consistent decline in mechanical properties. In the X direction, TPG shows a reduction in ultimate stress from 15.08 GPa to 9.47 GPa, while NTPG drops more sharply from 30.87 GPa to 18.38 GPa. A similar trend is observed across the Y direction, with TPG decreasing from 11.42 GPa to 9.29 GPa, and NTPG from 30.35 GPa to 22.69 GPa.

1. Introduction

The exploration of graphene and carbon allotropes has led to groundbreaking discoveries, including the synthesis of graphdiyne (GDY), a two-dimensional nanostructure composed of sp^2- and sp-hybridized carbon atoms [1–4]. Renowned for its exceptional mechanical strength, flexibility, and tunable electronic properties, GDY has emerged as a transformative material for applications in gas separation, catalysis, and biomedicine [5–8]. A significant advancement in this field is the development of nitrogen-doped GDY (N-GDY), where nitrogen atoms substitute carbon in the hexagonal lattice, enhancing its electronic and chemical reactivity [9–11]. This modification broadens GDY's utility in energy storage and catalysis while retaining its structural integrity [12–14].

Nikparsa et al. [15] investigated the maximum stress, strain, Young's modulus, and tensile toughness of NTPG nanosheets using classical molecular dynamics, incorporating factors such as temperature gradients, random defect densities, and geometric effects. Their results indicate that the NTPG nanosheet exhibits ultimate stresses of 31.24 GPa and 34.18 GPa, along with ultimate strains of 0.10 and 0.12, in the X and Y directions, respectively.

Further innovation in the GDY family arose with the experimental synthesis of triphenylene-based graphdiyne (TPG) by Matsuoka et al. [16] This material, featuring a unique porous architecture with extended carbon chains, demonstrates remarkable potential as an anode for batteries and energy storage systems [17]. Building on this, Kan et al. [18] pioneered nitrogen-doped TPG (NTPG) through theoretical studies, revealing enhanced mechanical and electronic properties via molecular dynamics (MD) and density functional theory (DFT) simulations [19–21].

Mortazavi et al. [22] investigated the thermal stability, electronic, mechanical, and optical properties of single-layer TPG and NTPG. They reported maximum tensile strengths of 8.47 N/m and 7.70 N/m for TPG and NTPG in the armchair direction, and 11.95 N/m and 10.37 N/m in the zigzag direction, respectively. Young's modulus values were found to be 87.8 N/m (TPG) and 93.4 N/m (NTPG) in the zigzag direction, and 87.9 N/m (TPG) and 92.5 N/m (NTPG) in the armchair direction. The ultimate strain values for TPG were 0.14 (armchair) and 0.18 (zigzag), whereas for NTPG, these values were 0.14 (zigzag) and 0.12 (armchair).

Salavati et al. [23] explored the potential of NTPG as an anode material for Li-ion batteries and extended their investigation to sodium (Na), potassium (K), magnesium (Mg), and calcium (Ca) storage. Their results indicated that NTPG nanosheets maintain structural stability during ion storage, even at temperatures as high as 2000 K. Also, Hatam-Lee et al. [10] studied the thermal conductivity and mechanical properties of 15 graphene-based materials, including TPG and NTPG. They reported Young's moduli of 189 GPa (X) and 147 GPa (Y) for TPG, and 251 GPa (X) and 227.2 GPa (Y) for NTPG.

Functionalization is a powerful strategy for tailoring the mechanical, electronic, and chemical properties of graphdiyne (GDY) and designing novel carbon allotropes. Hydrogenated GDY, for instance, exhibits tunable properties as demonstrated in prior studies [24,25]. Recent research has confirmed that hydrogen atoms and hydroxyl (OH) groups significantly influence GDY's properties. Through molecular dynamics (MD) simulations of GDY hydrogenation, Autreto et al. [26] identified preferential hydrogen bonding to butadiynic carbon atoms during GDY hydrogenation, followed by single-bonded carbons. Tan et al. [27] confirmed this adsorption hierarchy at low coverage, while Rouhi et al. [28] observed a reduction in elastic modulus with increasing hydrogen coverage.

The unique architecture of triphenylene graphdiyne (TPG) and nitrogen-doped TPG (NTPG), characterized by extended carbon chains, low density, and nanoscale voids, offers both advantages and challenges for hydrogen functionalization. These structural features inherently weaken the bonding network and introduce mechanical instability, making systematic functionalization computationally demanding. In this study, we present the first comprehensive molecular dynamics (MD) investigation of hydrogen-functionalized TPG and NTPG nanosheets under uniaxial tensile loading. Hydrogen atoms were randomly distributed across both surfaces to simulate realistic adsorption conditions. Our results demonstrate that increasing the degree of hydrogen functionalization (from 2.5 % to 10 %) causes a consistent decline in mechanical properties including Young's modulus, failure stress, failure strain, and tensile toughness in both TPG and NTPG. Also in this work compressive study of the effect of nitrogen doping on the nanosheets, during increasing the functionalization percentage have been conducted. These findings offer valuable insights into the mechanical behavior of covalently modified low-density carbon frameworks and provide a foundation for guiding the design and application of functionalized TPG-based nanosheets in nanomechanical and nanoelectronic systems.

The paper is structured as follows: Section 2 details the MD methodology and computational models. Section 3 examines tensile behavior across functionalization percentages (2.5 %, 5 %, 7.5 %, 10 %), quantifying Young's modulus, failure stress/strain, tensile toughness, and failure initiation points. Section 4 concludes with key findings and implications.

2. Methodology

The simulations were performed by numerically solving Newton's equations of motion. For each atom, the force fields were calculated as the gradients of the potential energy. These forces were then incorporated into Newton's equations and iteratively integrated over time using numerical methods. In this study, the classical molecular dynamics (MD) method was employed to simulate the behavior of nanostructures. The simulations were conducted using the LAMMPS code, a widely used classical molecular dynamics simulation package [29]. The LAMMPS simulation code has been widely utilized in different studies in recent years [30–34]. LAMMPS simulations involve accurate modeling the motions and interactions of all atoms within a structure.

For the energy expressions associated with the modeled TPG nanosheet, the Tersoff potential is employed to model intra-layer interactions within the TPG. On the other hand, the interactions at the site of functionalization are described by the Dreiding force field [37] for C and H atoms, supplemented by the Lennard-Jones (LJ) potential (implemented as lj/cut with a cutoff radius of 10 Å). The relevant LJ coefficients for hydrogen and carbon were derived from Mayo [37]. By combining Tersoff and Dreiding [35,36], these simulations achieve a balance of accuracy, computational efficiency, and physical realism tailored to the hybrid nature of this nanostructure. Also, the same method was applied for NTPG. In this case, the Tersoff potential suitably described the interaction between carbon and nitrogen atoms and the hydrogen-functionalized atoms on the top and bottom surfaces, described by Dreiding and LJ coefficients. The standard form of the

Table 1
Mechanical properties of the hydrogen-functionalized TPG nanosheet under uniaxial tension for three different displacement increments (0.01 Å/step, 0.02 Å/step, and 0.03 Å/step). The table reports the corresponding ultimate stress and strain values, along with the percentage error relative to the value of 0.02 Å/step.

Properties	Displace Value = 0.03	Displace Value = 0.02	error(%)
Max. Stress (GPa)	10.91	11.42	4.46
Max. Strain	0.071	0.074	4.06
Properties	Displace Value = 0.01	Displace Value = 0.02	error(%)
Max. Stress (GPa)	11.77	11.42	2.97
Max. Strain	0.077	0.074	3.89

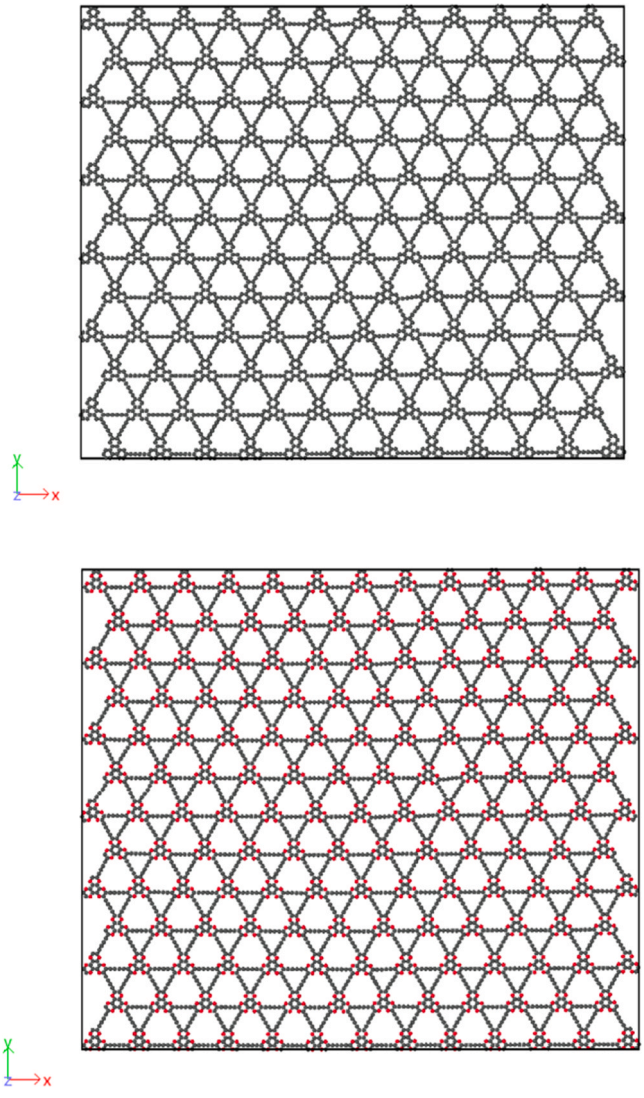

Fig. 1. Front views of TPG and NTPG nanosheets: (a) TPG nanosheet with carbon atoms shown in dark gray; (b) NTPG nanosheet with carbon atoms shown in dark gray and nitrogen atoms in red.

Table 2
The dimension of the TPG and NTPG nanosheets (Å) in the X (length) and Y (width) directions.

Nanosheet	Length (Å)	Width(Å)
TPG	184.5	154.5
NTPG	194	167.5

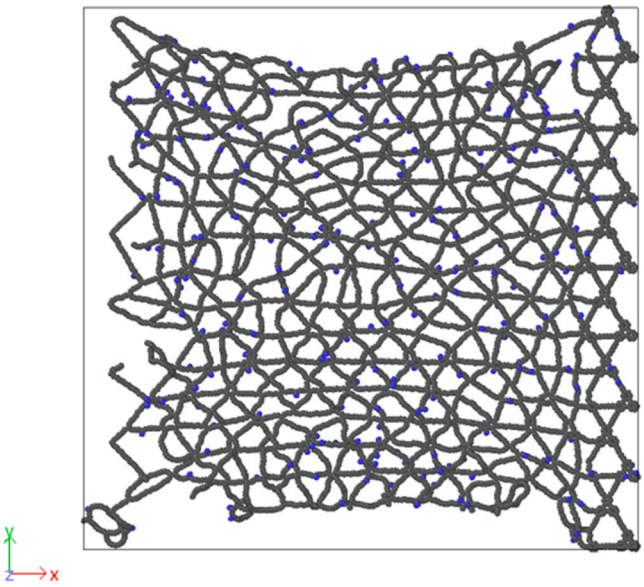

Fig. 2. The front view of the TPG nanosheet functionalized with 5 % hydrogen, dark gray atoms represent carbon, while blue atoms indicate hydrogen.

Dreiding force field comprises energy expressions that compute the potential energy associated with the valence and non-bonded interactions. The potential energy terms are calculated as:

$$E_{potential} = E_{valance} + E_{nonbonded} \quad (1)$$

$$E_{valance} = E_{bond} + E_{angle} + E_{torsion} + E_{inversion} \quad (2)$$

$$E_{nonbonded} = E_{vdWaals} + E_{electrostatic} + E_{hydrogen\ bond} \quad (3)$$

The potential energy terms related to the bond stretching (E_{bond}), bond-angle bending (E_{angle}), dihedral angle torsion ($E_{torsion}$), and $E_{inversion}$ are presented:

$$E_{bond} = \frac{1}{2} K_b (R - R_0)^2 \quad (4)$$

$$E_{angle} = \frac{1}{2} C_{IJK} \left(\cos\theta_{IJK} - \cos\theta_j^0 \right)^2 \quad (5)$$

$$E_{torsion} = \frac{1}{2} V_{JK} \{1 - \cos[n_{JK}(\varnothing - \varnothing_{JK}^0)]\} \quad (6)$$

$$E_{inversion} = \frac{1}{2} C_1 \left(\cos\varphi - \cos\varphi_j^0 \right)^2 \quad (7)$$

While K_b, C_{IJK}, V_{JK}, C_1 illustrates the bond energy's force constant and angle energy's force constant, the barrier to rotation, and the parameter corresponding to the force constant for the inversion term, in order. The R, θ_{IJK}, $\varnothing$, and φ parameters demonstrate the length of the bond, bond angle, torsion angle (dihedral angle), and inversion angle (angle between the JIK plane and IL bond), correspondingly, and the R_0, θ_j^0, $\varnothing_{JK}^0$, and φ_j^0 parameters refer to equilibrium values for bond length, bond angle, torsion angle, and inversion angle, respectively. Additionally, in the rotational potential, the number of minima is discovered by the periodicity of an integer parameter called n.

The van der Waals (vdW) interaction energy ($E_{vdWaals}$) is characterized by the L-J pair potential as:

$$E_{vdWaals} = 4\varepsilon \left[\left(\frac{\sigma}{r}\right)^{12} - \left(\frac{\sigma}{r}\right)^{6} \right] \quad (8)$$

Which in σ the length parameter, called the collision diameter, and the energy well depth are ε. To obtain the parameters of cross interactions, Lorentz–Berthelot mixing rules are used as below:

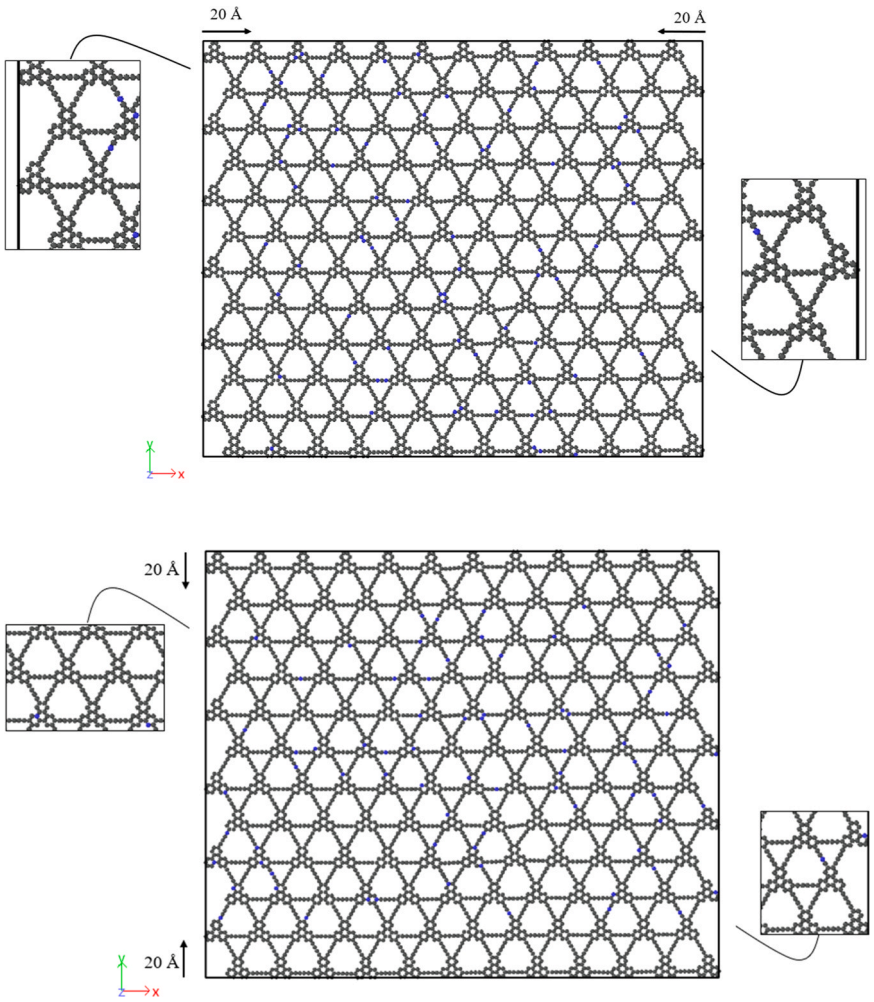

Fig. 3. A 20 Å-wide margin on both edges of the TPG nanosheet excluded from hydrogen functionalization, the dark gray represents carbon atoms and blue, hydrogen, (a) margin applied along the X-direction, (b) margin applied along the Y-direction.

$$\sigma_{ij} = \frac{\sigma_{ii} + \sigma_{jj}}{2} \tag{9}$$

$$\varepsilon_{ij} = \sqrt{\varepsilon_{ii}\varepsilon_{jj}} \tag{10}$$

The electrostatic and hydrogen bonding energies are explored by:

$$E_{electrostatic} = \frac{(322.0637)q_i q_j}{\varepsilon r_{ij}} \tag{11}$$

$$E_{hydrogen\ bond} = D_{hb}\left[5\left(\frac{R_{hb}}{R_{DA}}\right)^{12} - 6\left(\frac{R_{hb}}{R_{DA}}\right)^{10}\right]\cos^4(\theta_{DHA}) \tag{12}$$

In which q, ε, r_{ij}, D_{hb}, R_{hb}, R_{DA}, and θ_{DHA} parameters have been presented in detail in [31].

The minimization process is applied via the conjugate-gradient technique, and following that, the system undergoes a canonical ensemble (NVT) simulation at 300 K for 0.1 ns and with an integration time step of 0.001 ps. Employing the time step any numerically instable behavior of the system was noticed. In this step, the Nose–Hoover thermostat successfully controlled the thermodynamic fluctuation, allowing the structure to reach a stable equilibrium status. Following this, incrementally, a tensile displacement of 0.02 Å at each step on the boundaries. A relaxation process was applied at every step to minimize stress concentration. To verify that the selected displacement increment of 0.02 Å/step does not significantly influence the mechanical outcomes, we conducted a sensitivity analysis on a TPG structure functionalized with 2.5 % hydrogen under uniaxial tension along the Y-direction. Table 1 compares the maximum stress, maximum strain, and their relative errors for displacement steps of 0.01, 0.03 Å/step to 0.02. The results demonstrate that the deviations remain within 4.46 %, indicating that the chosen displacement step produces reliable and consistent mechanical responses. Based on this analysis, we adopted this displacement value for all simulations in this study, including those involving NTPG. Throughout the simulation, until failure occurred, the values, including potential energy, stress, and strain, were monitored by [38,39].

To construct the nanosheet models, BIOVIA Materials Studio [40] is employed. The front views of the unfunctionalized TPG and NTPG nanosheets are shown in Fig. 1. TPG nanosheet displaying carbon atoms in dark gray in Fig. 1a; NTPG nanosheet exhibiting carbon atoms in dark gray and nitrogen atoms in red presenting in Fig. 1b. The total number of atoms in the TPG and NTPG structures are 4131 and 4685, respectively. The dimensions of the nanosheets in the X and Y directions are listed in Table 2. A custom MATLAB script was developed to randomly distribute hydrogen atoms on both the top and bottom surfaces of the nanosheets, using a predefined H–C bond length, hydrogen atomic mass, and specified coverage percentages. In this study, hydrogen functionalization was applied at 2.5 %, 5 %, 7.5 %, and 10 % of the total number of atoms. These specific percentages were selected after extensive preliminary simulations and testing to ensure a representative range of functionalization effect. The selection of the 2.5 %–10 % hydrogen functionalization coverage range is supported by both theoretical considerations and

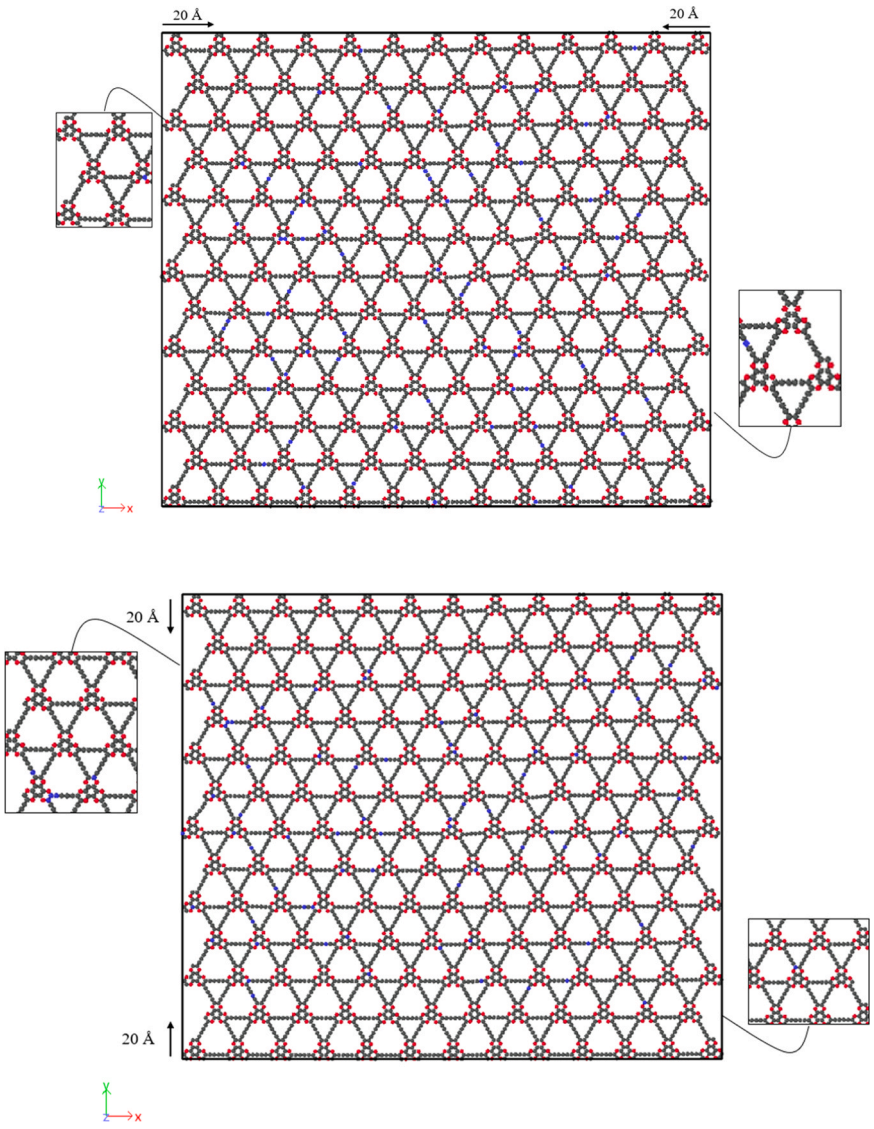

Fig. 4. A 20 Å-wide margin on both edges of the NTPG nanosheet excluded from hydrogen functionalization, the dark gray represents carbon atoms, red shows nitrogen and blue, displays hydrogen (a) margin applied along the X-direction, (b) margin applied along the Y-direction.

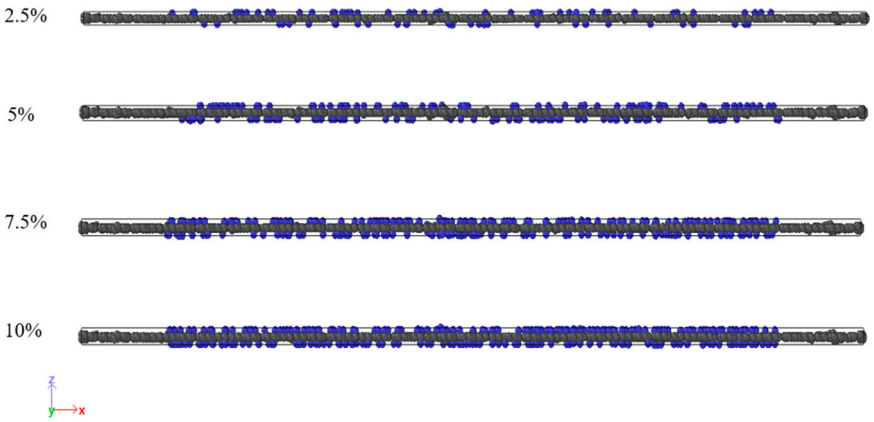

Fig. 5. Top views of the TPG nanosheet with randomly distributed hydrogen atoms at 2.5 %, 5 %, 7.5 %, and 10 % coverage on both the top and bottom surfaces, carbon atoms is shown with dark gray and hydrogen, with blue.

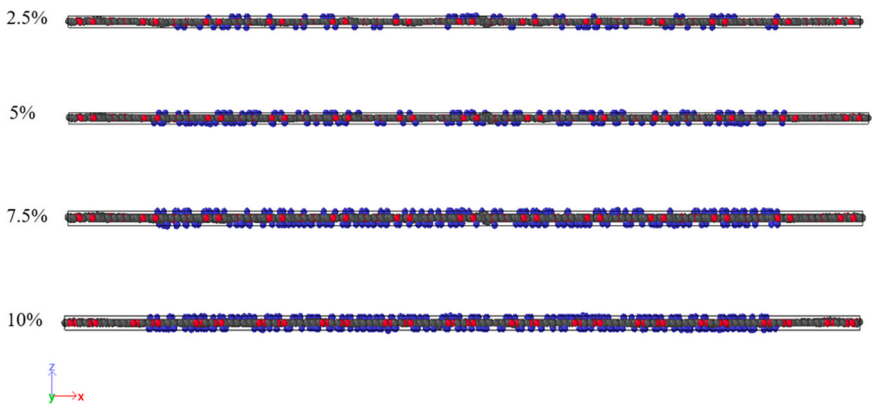

Fig. 6. Top views of the NTPG nanosheet with randomly distributed hydrogen atoms at 2.5 %, 5 %, 7.5 %, and 10 % coverage on both the top and bottom surfaces, carbon atoms is shown with dark gray, nitrogen with red and hydrogen, with blue.

experimental evidence. Preliminary simulations revealed that TPG and NTPG nanosheets maintain structural stability within this range, whereas coverages exceeding 10 % lead to high chance instability due to the conversion of sp^2 to sp^3 bonds, resulting in local distortion and mechanical weakening. Besides, the experimental studies confirm that the 2.5 %–10 % range is feasible and practical for TPG and NTPG, reinforcing the validity of our simulation results [41–43].

Hydrogen adsorption on the TPG and NTPG nanosheets turn sp or sp^2 carbon bonds into sp^3 C-H bonds, disrupting π-conjugation and opening band gaps. The lattice is weakening by these localized sp^3 sites; The hydrogenated C-C bonds are weaker, so denser hydrogen functionalized regions reduce stiffness and fracture at lower strain. Theoretical studies on graphene-family and carbon nanostructures consistently show that mechanical strength is significantly reduced by perturbing local electronic structure and that hydrogen passivation is a consequence of altering hybridization ($sp^2 \rightarrow sp^3$). In result, functionalizing near nanosheet edges and boundaries is avoided in practice, since hydrogen at those boundary sites would magnify fracture risk [44,45]. In our study, we observed that applying hydrogen functionalization near the boundaries of the nanosheets led to instability and, in some cases, structural collapse. This behavior was particularly evident when hydrogen atoms were randomly distributed on both the top and bottom surfaces of the porous nanosheets. Through multiple test simulations, it is determined that, for the given nanosheet size and physical conditions, leaving a 20 Å-wide margin on both edges, free of hydrogen functionalization, significantly improved the structural integrity under tensile loading. Accordingly, in the direction of the applied tensile strain, this unfunctionalized boundary region was preserved. This strategy enhanced the mechanical stability of the nanosheets and allowed them to better withstand and simulate the tensile stress conditions.

Fig. 2. Front view of a TPG nanosheet with 5 % hydrogen coverage, shown without the 20 Å hydrogen-free margins. Carbon atoms are in dark gray and hydrogen in blue. The structure collapses after minimization and early tensile loading due to hydrogenation near the boundaries, which induces local strain and instability. This highlights the need for excluding functionalization at the edges to preserve structural integrity during simulation. To ensure structural integrity and minimize edge effects during mechanical testing, a 20 Å-wide margin was applied to both edges of the TPG and NTPG nanosheets, excluding these regions from hydrogen functionalization. This margin was systematically applied in two orientations: along the X-direction and Y-direction, as illustrated in, Figs. 3 and 4. For the TPG nanosheets (Fig. 3), the structural representation shows carbon atoms in dark gray and hydrogen atoms in blue, with the protected edge regions clearly demarcated in both Fig. 3.a X-direction and Fig. 3.b Y-direction configurations. Similarly, for the NTPG nanosheets (Fig. 4), carbon atoms are displayed in dark gray, nitrogen atoms in red, and hydrogen atoms in blue, with the same 20 Å margin protocol applied along the X and Y-direction. This edge exclusion strategy prevents potential artifacts arising from boundary conditions and ensures that the hydrogen functionalization occurs only within the stable interior regions of the nanosheets, thereby providing more reliable mechanical property assessments under tensile loading conditions.

The 20 Å hydrogen-free boundary margin methodology employed in this study represents a generalizable approach for investigating functionalized 2D materials while preserving their intrinsic mechanical properties. This methodology is particularly valuable for porous 2D materials where edge sensitivity can significantly impact mechanical response characterization [46–49].

To provide further clarity on the random distribution of hydrogen atoms on the nanosheet surfaces, Figs. 5 and 6 present comprehensive top views of representative configurations at various functionalization levels. Fig. 5 displays the TPG nanosheet with randomly distributed hydrogen atoms at 2.5 %, 5 %, 7.5 %, and 10 % coverage levels, where the structures are oriented along the X-direction with carbon atoms shown in dark gray and hydrogen atoms in blue. The progressive increase in hydrogen coverage is clearly visible across the four configurations, demonstrating the systematic nature of the functionalization process while maintaining the random spatial distribution of hydrogen atoms across the nanosheet surface. Similarly, Fig. 6 shows the corresponding top views for NTPG nanosheets under identical functionalization conditions, with carbon atoms displayed in dark gray, nitrogen atoms in red, and hydrogen atoms in blue. These visual representations illustrate how the hydrogen atoms are uniformly dispersed across both the top and bottom surfaces of the nanosheets.

In addition, with the aid of VMD (Visual Molecular Dynamics) software [50,51], coordinate data suitable for LAMMPS simulations were generated. OVITO (Open Visualization Tool, [52]) was also used for visualization and monitoring of the tension distribution across the nanosheets. All results presented in this study represent the average values obtained from five independent simulation runs for each level of hydrogen functionalization in the uniaxial loading direction.

Mechanical properties including failure stress, failure strain, Young's modulus, and tensile toughness were evaluated and analyzed. Stress–-strain curves were plotted up to the point of structural failure for each configuration. Young's modulus was extracted by calculating the slope of the linear portion of the stress–strain curve up to 3 % strain. Tensile toughness was obtained as the area under the stress–strain curve, while the drop in stress was used to identify the failure stress and strain. The values presented in this study represent the average results from five random distributions of hydrogen atoms.

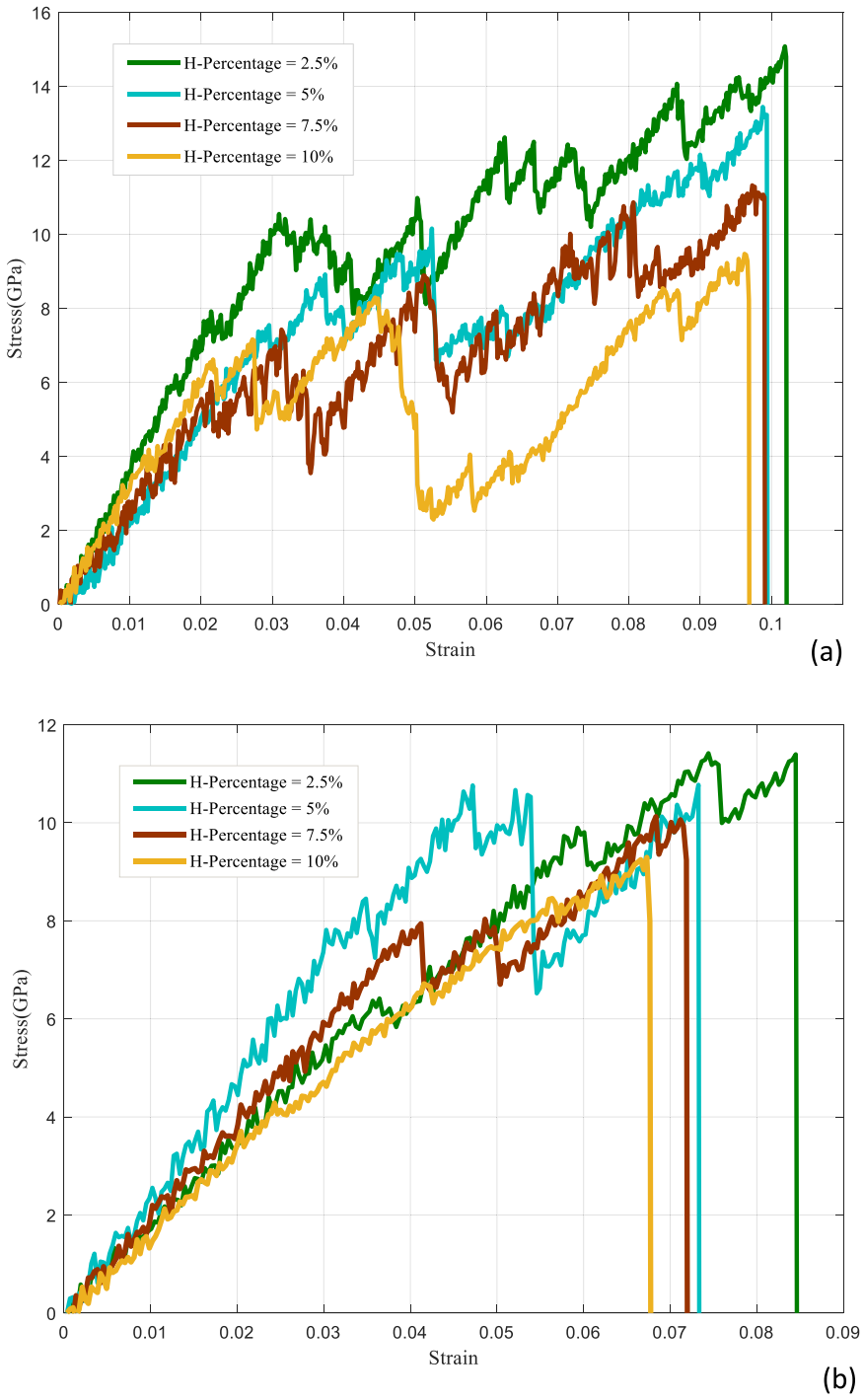

Fig. 7. Stress-strain curve for TPG nanosheet applying H- functionalization (2.5 %, 5 %, 7.5 %, and 10 %): (a) in the X direction; (b) in the Y direction.

3. Results and discussion

In this section, the mechanical properties of TPG, NTPG under random hydrogen functionalization are discussed. These properties, derived from the stress-strain relationship, include ultimate stress, ultimate strain, elastic modulus, and tensile toughness. The nanosheets were subjected to uniaxial tensile loading. All simulations in this study were conducted using molecular dynamics. The hydrogen functionalization was applied at concentrations of 2.5 %, 5 %, 7.5 %, and 10 % of the total number of atoms in each structure.

Fig. 7 presents the stress-strain curves for the TPG nanosheet under hydrogen functionalization at concentrations of 2.5 %, 5 %, 7.5 %, and 10 %. As shown in Fig. 7a, the nanosheet is subjected to tensile tension in the X-direction. With increasing hydrogen functionalization, the ultimate stress and strain of the nanosheet decrease, indicating that the material becomes weaker and less capable of withstanding external forces. This leads to failure at lower stress levels. The introduction of hydrogen atoms weakens the bonds within the nanosheet, significantly compromising its structural integrity. Fig. 7b illustrates the stress-strain curve for the TPG nanosheet under hydrogen functionalization when tensile tension is applied in the Y-direction. As the degree of functionalization increases, the maximum stress and strain values decline, resulting in earlier failure. The hydrogen functionalization introduces defects into the porous structure of the nanosheet, further weakening the

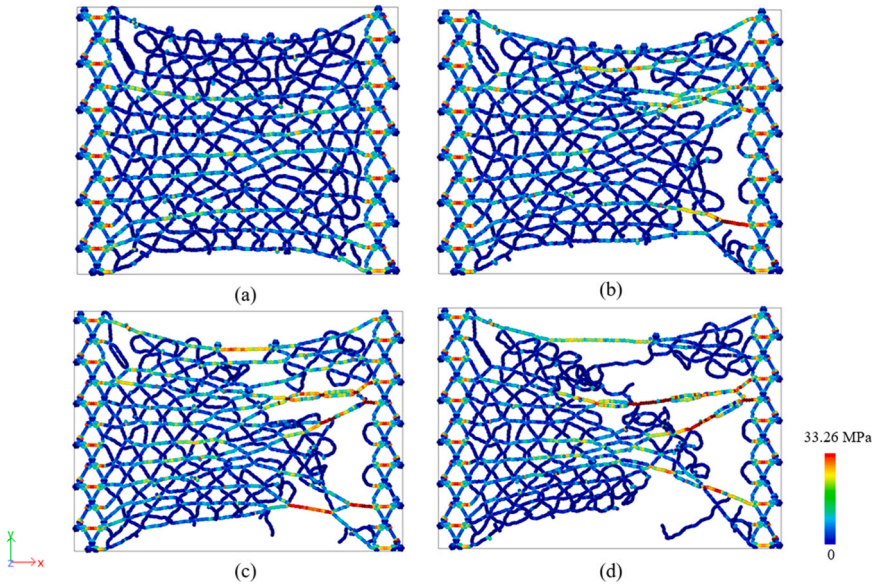

Fig. 8. Depicts the failure location of the TPG nanosheet under tensile loading in the X direction. (a) to (c) illustrate the stress distribution and the progression of failure during the application of tension in the X direction. (d) shows the nanosheet immediately after failure, highlighting the structural breakdown caused by the applied tension.

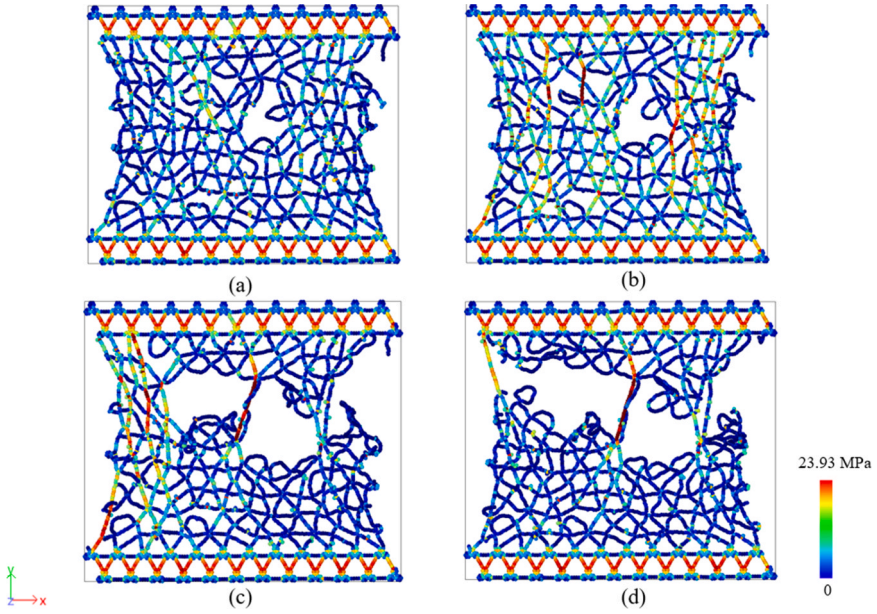

Fig. 9. Depicts the failure location of the TPG nanosheet under tensile loading in the Y direction. (a) to (c) illustrate the stress distribution and the progression of failure during the application of tension in the Y direction. (d) shows the nanosheet immediately after failure, highlighting the structural breakdown caused by the applied tension.

bonds and reducing its overall integrity.

Fig. 8 illustrates the tension distribution in the 2.5 % H-functionalized TPG nanosheet along the X-direction. As depicted in Fig. 8a, hydrogen functionalization introduces defects into the porous nanosheet. These defects, caused by bond weakening and structural vacancies, lead to a continuous but rapid decline in the nanosheet's stress and strain performance. However, due to the inherent stretchability of the nanosheet, it can sustain tension until reaching its ultimate stress and strain, as shown in Fig. 8b and c, respectively. While the bonds surrounding the defects exhibit higher endurance, the nanosheet ultimately undergoes failure, as illustrated in Fig. 8d.

Fig. 9 provides a comprehensive visualization of the mechanical failure process in a 5 % hydrogen-functionalized TPG nanosheet subjected to tensile loading along the Y-direction. The figure illustrates the progressive evolution of stress distribution and structural degradation through four distinct stages of the failure mechanism. In the initial stage (Fig. 9a), the stress distribution is relatively uniform across the nanosheet, with localized stress concentrations beginning to develop around hydrogen functionalization sites, which act as structural weak points due to the disruption of the pristine carbon network. As the tensile load continues to increase (Fig. 9b), these stress concentrations intensify and begin to propagate, leading to the initiation of bond breaking in regions of highest stress density. The hydrogen functionalization sites serve as nucleation points for crack formation, as the sp^3 hybridization of carbon atoms bonded to hydrogen atoms creates local distortions in the otherwise planar sp^2 carbon framework.

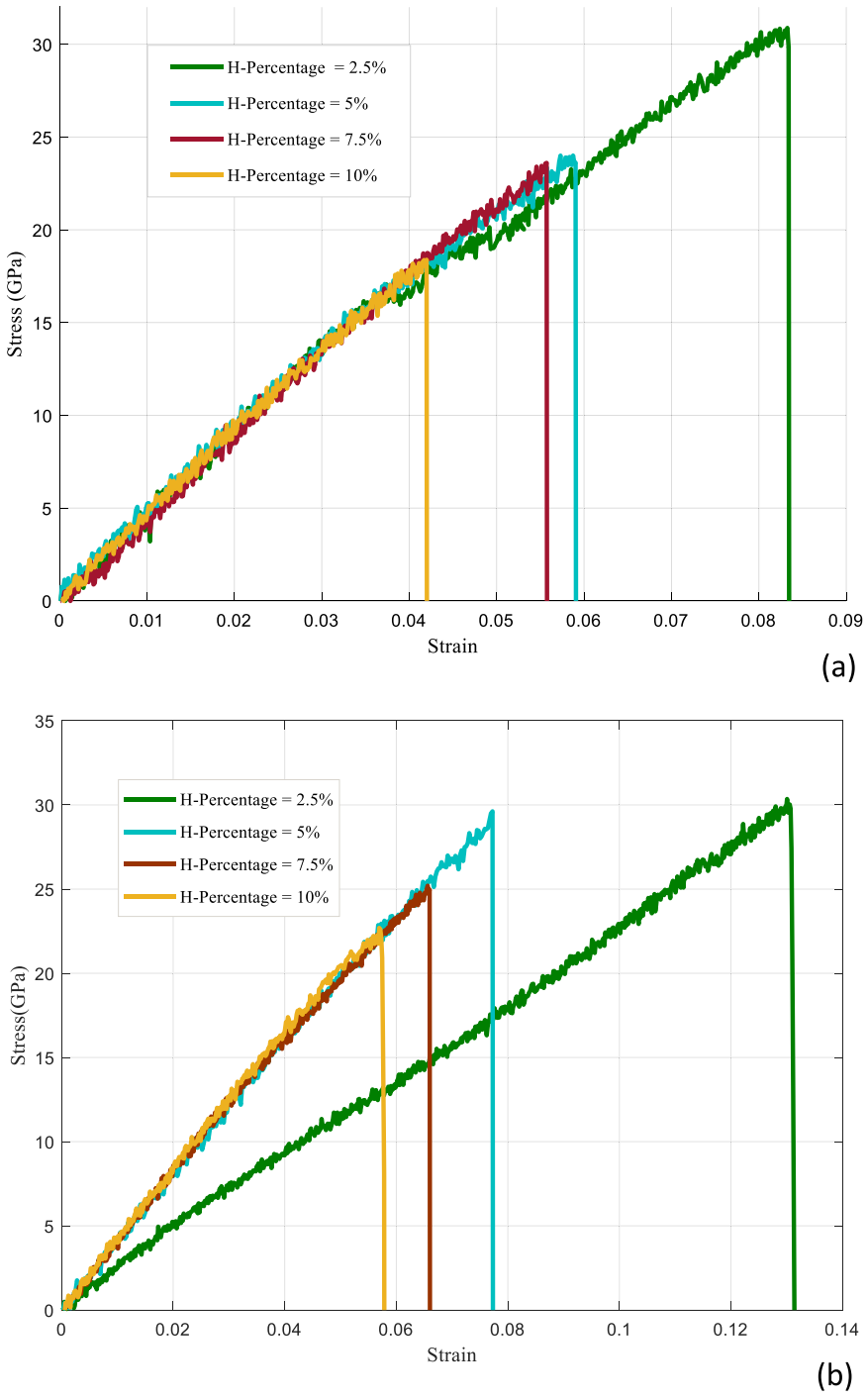

Fig. 10. Stress-Strain curve for NTPG nanosheet applying H- functionalization (2.5 %, 5 %, 7.5 %, and 10 %): (a) in the X direction; (b) in the Y direction.

The progression of failure becomes more pronounced in Fig. 9c, where significant structural damage is evident as cracks propagate through the nanosheet in a non-uniform manner. The final stage (Fig. 9d) shows the nanosheet immediately after complete failure, highlighting the catastrophic structural breakdown caused by the applied tension. The failure pattern exhibits characteristics of brittle fracture during the tensile tension in the Y direction.

Fig. 10 illustrates the stress-strain curves for the NTPG nanosheet under hydrogen functionalization at concentrations of 2.5 %, 5 %, 7.5 %, and 10 % of the total number of atoms. Fig. 10a shows the nanosheet subjected to tensile tension in the X-direction. As the hydrogen functionalization increases, the failure stress and strain of the nanosheet decrease, leading to failure at lower stress levels. Similar to the TPG nanosheet, the introduction of hydrogen atoms weakens the bonds within the NTPG nanosheet, compromising its structural integrity. Fig. 10b illustrates the stress-strain curve for the NTPG nanosheet under hydrogen functionalization when tensile tension is applied in the Y-direction. As the degree of functionalization increases, the maximum stress and strain values decline, resulting in earlier failure. Similar to the TPG nanosheet, hydrogen functionalization introduces defects into the porous structure of the NTPG nanosheet, further weakening the bonds and reducing its overall integrity.

Fig. 11 shows the tension distribution for the NTPG nanosheet under tensile tension in the X-direction with 5 % hydrogen functionalization

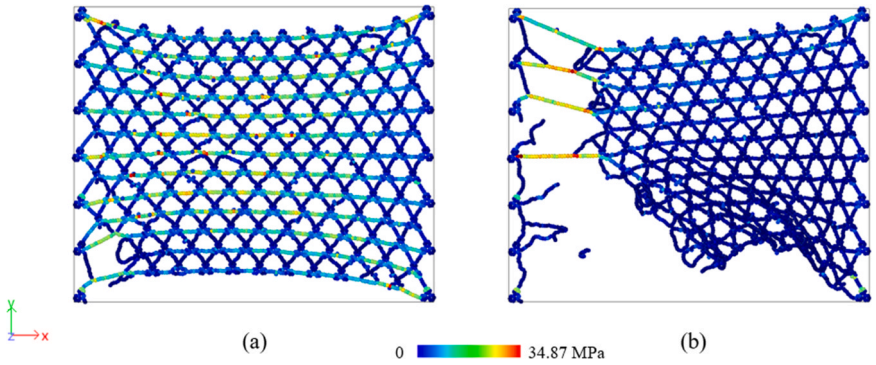

Fig. 11. Presents the stress distribution of the NTPG nanosheet under tensile loading in the X direction. (a) NTPG under tension displacement just before the ultimate failure, (b) NTPG just after the ultimate failure.

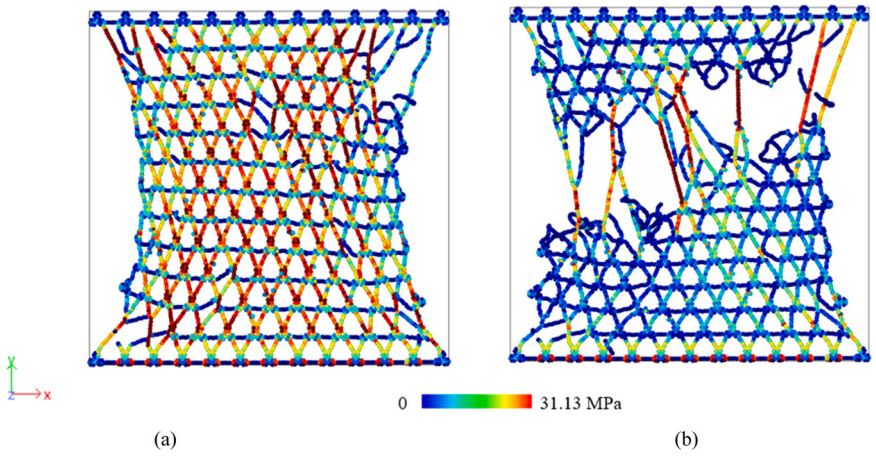

Fig. 12. Presents the stress distribution of the NTPG nanosheet under tensile loading in the Y direction: (a) NTPG under tension displacement just before the ultimate failure; (b) NTPG just after the ultimate failure.

Table 3
The hydrogen functionalization including (2.5 %, 5 %, 7.5, and 10 %), elastic modulus, ultimate stress, ultimate strain, and toughness for the TPG nanosheet in the X and Y directions.

X Direction				
H-Functionalization (%)	Young's Modulus (GPa)	Failure Stress (GPa)	Failure Strain	Tensile Toughness (GPa)
2.5	132.82	15.0779	0.1019	0.96
5	118.3	13.4407	0.0988	0.7414
7.5	114.13	11.3213	0.0973	0.6542
10	81.72	9.4702	0.0962	0.5217
Y Direction				
H-Functionalization (%)	Young's Modulus (GPa)	Failure Stress (GPa)	Max Strain	Tensile Toughness (Gpa)
2.5	129.4714	11.4173	0.0744	0.5518
5	122.0288	10.7735	0.0733	0.4866
7.5	124.0559	10.125	0.0683	0.4135
10	121.7373	9.2948	0.0673	0.3425

Table 4
The hydrogen functionalization including (2.5 %, 5 %, 7.5, and 10 %), elastic modulus, ultimate stress, ultimate strain, and toughness for the NTPG nanosheet in the X and Y directions.

	X Direction			
H-Functionalization (%)	Young's Modulus (GPa)	Failure Stress (GPa)	Failure Strain	Tensile Toughness (GPa)
2.5	309.73	30.87	0.083	1.52
5	299.48	23.99	0.059	0.83
7.5	229.49	23.6	0.056	0.73
10	193.04	18.38	0.042	0.43
	Y Direction			
H-Functionalization (%)	Young's Modulus (GPa)	Failure Stress (GPa)	Max Strain	Tensile Toughness (GPa)
2.5	220.06	30.3473	0.1301	1.95
5	217.4	29.6153	0.0772	1.18
7.5	197.81	25.1943	0.0653	0.86
10	180.16	22.6918	0.057	0.68

applied. Fig. 11a illustrates the tension distribution just before ultimate failure. Due to hydrogen functionalization, defects and vacancies occur in the nanosheet, weakening the bonds and reducing its structural integrity. Fig. 11b depicts the nanosheet immediately after failure. Fig. 12 displays the tension distribution for the NTPG nanosheet under tensile tension in the Y-direction with 2.5 % hydrogen functionalization applied. Fig. 12. a shows the tension distribution just before ultimate failure. The failure initiates from the upper-right vacancy, a consequence of hydrogen functionalization, and continuously propagates to other vacancies in the nanosheet, ultimately leading to complete failure as shown in Fig. 12b.

Table 3 summarizes the mechanical properties of TPG nanosheets in the X and Y directions, including first failure stress, first failure strain, Young's modulus, and tensile toughness. Table 4 presents the corresponding properties for NTPG.

In Table 3, as the degree of hydrogen functionalization increases in

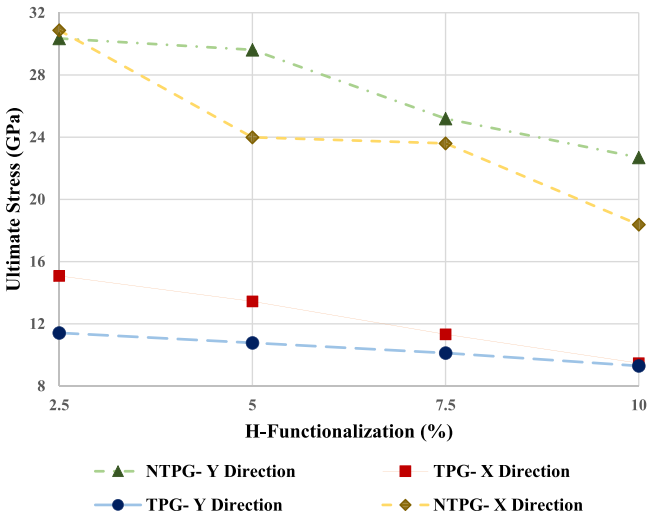

Fig. 13. Ultimate stress values for hydrogen functionalization percentages of 2.5 %, 5 %, 7.5 %, and 10 % in TPG and NTPG under uniaxial tensile loading. The TPG results are shown in red for the X direction and blue for the Y direction, while the NTPG results are represented in yellow for the X direction and green for the Y direction.

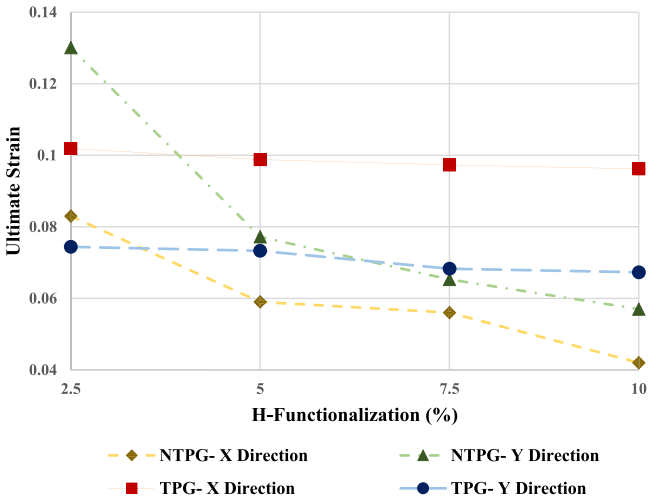

Fig. 14. Ultimate strain values for hydrogen functionalization percentages of 2.5 %, 5 %, 7.5 %, and 10 % in TPG and NTPG under uniaxial tensile loading. The TPG results are shown in red for the X direction and blue for the Y direction, while the NTPG results are represented in yellow for the X direction and green for the Y direction.

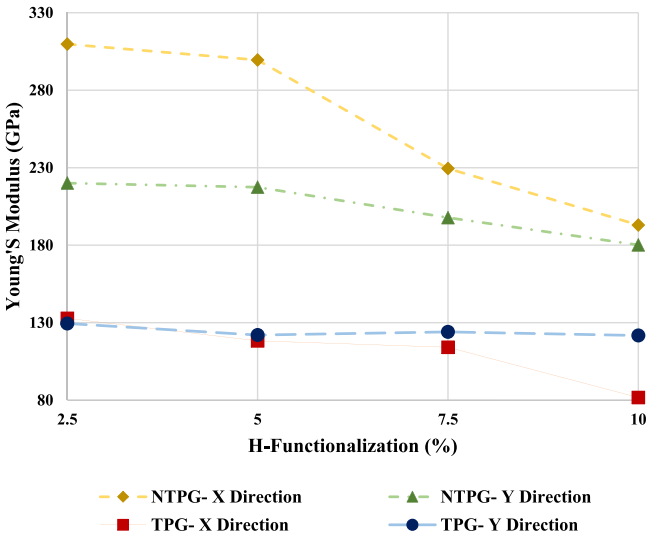

Fig. 15. Comparison of Young's modulus for TPG and NTPG nanosheets under uniaxial tension at hydrogen functionalization levels of 2.5 %, 5 %, 7.5 %, and 10 %. TPG data are shown in red (X direction) and blue (Y direction), while NTPG data appear in yellow (X direction) and green (Y direction).

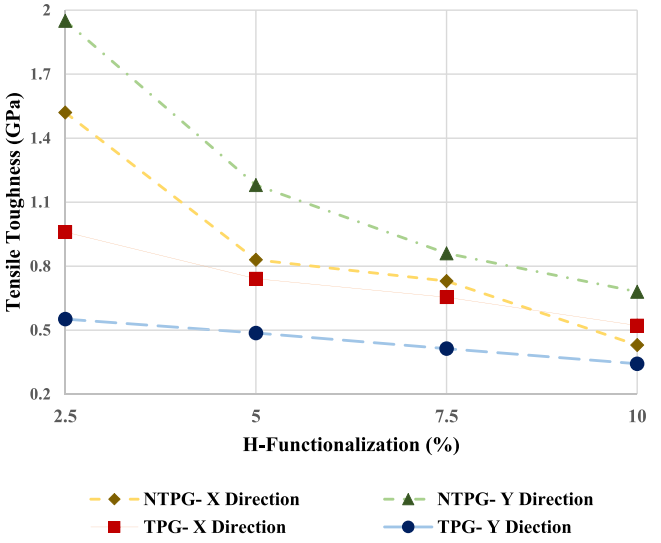

Fig. 16. Tensile toughness for TPG and NTPG nanosheets under uniaxial loading at hydrogen functionalization levels of 2.5 %, 5 %, 7.5 %, and 10 %. Red and blue lines represent TPG in the X and Y directions, respectively, while yellow and green lines indicate NTPG in the X and Y directions.

the X direction, Young's modulus decreases. For example, at 7.5 % functionalization, Young's modulus is 114.13 GPa, compared to 118.3 GPa at 5 %. Both the first failure stress and ultimate failure stress also decline with increased functionalization. At 10 %, these values drop to 9.47 GPa and 0.096 GPa, respectively, while at 2.5 % they are 15.08 GPa and 0.10 GPa. Tensile toughness also decreases, from 0.96 GPa at 2.5 % to 0.65 GPa at 7.5 %. A similar trend is observed in the Y direction. From 2.5 % to 10 % functionalization, ultimate stress, ultimate strain, Young's modulus, and tensile toughness decrease by approximately 2.12 GPa, 0.007, 7.73 GPa, and 0.21, respectively.

In Table 4, for NTPG under tensile loading in the X direction, the ultimate stress shows a reduction of approximately 12.49 GPa from 2.5 % to 10 % functionalization. Failure strain also decreases slightly, with a difference of 0.041 between 2.5 % and 10 %. Young's modulus follows a similar trend for instance, it is 309.73 GPa at 7.5 %, compared to 299.48 GPa at 5 %. Toughness also declines with increasing functionalization, with values of 1.52 and 0.73 (in GPa) at 2.5 % and 7.5 %, respectively. The Y direction exhibits the same general trend. From 2.5 % to 10 % functionalization, the ultimate stress, ultimate strain, Young's modulus, and tensile toughness decrease by approximately 7.65 GPa, 0.0731,39.9 GPa and 1.27 GPa, respectively.

Our molecular dynamics results show that hydrogen functionalization dramatically weakens both materials. In all cases, increasing H coverage from 2.5 % to 10 % results in a monotonic decrease in Young's modulus, failure stress, failure strain, and toughness for both TPG and NTPG.

Previous studies have shown that nitrogen doping significantly enhances the stiffness and strength of triphenylene-graphdiyne (TPG). Mortazavi et al. [22] predicted that N-doped TPG (NTPG) remains elastically stiff and can sustain high tensile stress, exhibiting linear elastic behavior with considerable strength [22]. In line with this, Hatam-Lee et al. [10] reported much higher Young's moduli for NTPG

(approximately 251 GPa in X and 227 GPa in Y) compared to TPG (≈189 GPa in X and 147 GPa in Y). Nikparsa et al. [15] similarly showed that NTPG monolayers can withstand ultimate stresses of 31–34 GPa and failure strains of around 0.10–0.12. Collectively, these works demonstrate that NTPG is substantially stronger and stiffer than TPG under tensile loading, due to the reinforcing effect of nitrogen doping.

Fig. 13 shows the maximum stress values for TPG and NTPG nanosheets under various levels of hydrogen functionalization (2.5 %, 5 %, 7.5 %, and 10 %) in both directions. At 2.5 % hydrogen functionalization, the TPG nanosheet has a maximum stress of 15.08 GPa in the X direction and 11.42 GPa across the Y direction. In contrast, NTPG reaches 30.87 GPa (X) and 30.35 GPa (Y), showing a clear enhancement. The absolute increases are 15.79 GPa in X and 18.93 GPa in Y compared to TPG. These results confirm that nitrogen doping significantly reinforces the tensile strength of the graphdiyne lattice, particularly in the Y direction. Among all cases, the 2.5 % functionalized NTPG (X) shows the highest stress value, while the TPG (Y) exhibits the lowest. Additionally, hydrogen functionalization has a more intense weakening effect on NTPG than on TPG, indicating a steeper decline in strength with increasing functionalization.

Fig. 14 presents the ultimate strain values for TPG and NTPG nanosheets under various hydrogen functionalization levels. The results reveal anisotropic behavior. In the X direction, TPG exhibits superior ductility at 2.5 % H-functionalization with a strain of 0.1019, surpassing NTPG (X) at 0.083 by roughly 23 %. Conversely, in the Y direction, nitrogen doping enhances ductility: NTPG (Y) reaches 0.1301, compared to TPG (Y) at 0.0744. Except at 2.5 %, TPG (X) consistently shows the highest strain, while NTPG (X) presents the lowest.

Fig. 15 displays the Young's modulus values for both nanosheets across different hydrogen functionalization levels. At 2.5 % functionalization, TPG shows 132.82 GPa (X) and 129.47 GPa (Y), whereas NTPG reaches 309.73 GPa (X) and 220.06 GPa (Y), reflecting significant improvements due to nitrogen doping. These enhancements highlight how nitrogen atoms strengthen nanosheet stiffness, especially in the X direction where atomic bonding is more efficient. Among all cases, NTPG (X) exhibits the highest stiffness, while TPG (X) presents the lowest (except at 2.5 %, where TPG (X) is slightly higher than TPG (Y)).

Fig. 16 illustrates the tensile toughness values for TPG and NTPG. At 2.5 % hydrogen functionalization, TPG has toughness values of 0.96 (X) and 0.552 (Y), while NTPG exhibits 1.52 (X) and 1.95 (Y). Nitrogen doping thus results in substantial improvements, an increase of 0.56 in the X direction and 1.398 in the Y direction. While TPG shows higher toughness in the X direction, NTPG displays greater toughness in the Y direction. Furthermore, hydrogen functionalization leads to a sharper decline in toughness for NTPG than for TPG, but overall, NTPG (Y) remains the toughest and TPG (Y) the least.

The incorporation of nitrogen atoms into the NTPG structure fundamentally alters its electronic and bonding properties compared to TPG. Nitrogen, with its additional valence electron, introduces sites of heightened reactivity within the NTPG lattice. This increased reactivity makes NTPG more susceptible to hydrogen attachment during functionalization, leading to stronger or more extensive bonding between hydrogen and the nitrogen-doped sites. As a result, the structural integrity and mechanical properties of NTPG are more severely compromised under hydrogenation compared to TPG, which exhibits a more stable and gradual response due to its uniform carbon-based composition [53–55].

4. Conclusion

The presented research study carried out the first MD investigation of hydrogen-functionalized TPG and NTPG under tensile loading, revealing the impact of functionalization on the attributed mechanical performance. Based upon the proposed computational approach, which includes a novel hydrogen-free boundary margin, it was possible to improve the stability of modeled structures as well as to prevent the premature failure. The extracted numerical results demonstrated that hydrogen coverage considerable influences on the mechanical behavior, including failure stress and strain, Young's modulus, and toughness of TPG as well as NTPG nanosheets. Specifically, it was observed that:

- At 2.5 % hydrogen functionalization, the TPG nanosheet has a maximum stress of 15.08 GPa across the X direction and 11.42 GPa along with the Y direction. In contrast, NTPG reaches 30.87 GPa in X direction and 30.35 GPa across the Y axis, showing a clear enhancement. These results confirm that nitrogen doping significantly reinforces the tensile strength of the graphdiyne lattice, particularly in the Y direction.
- The results revealed anisotropic behavior for the both TPG and NTPG nanosheets. In the X direction, TPG exhibits superior ductility at 2.5 % hydrogen functionalization with a strain of 0.1019, surpassing NTPG (X) at 0.083 by roughly 23 %. Conversely, in the Y direction, nitrogen doping enhances ductility: NTPG (Y) reaches 0.1301, compared to TPG (Y) at 0.0744. Except at 2.5 %, TPG (X) consistently shows the highest strain, while NTPG (X) presents the lowest.
- It was found that increasing hydrogen functionalization from 2.5 % to 10 % leads to a consistent decline in all mechanical properties for both TPG and NTPG. Despite NTPG exhibiting superior mechanical performance compared to TPG at low functionalization levels reaching up to 30.87 GPa ultimate stress and 309.73 GPa Young's modulus its mechanical properties deteriorate more rapidly with increased hydrogen coverage. For instance, NTPG's tensile toughness in the X direction drops from 1.52 GPa at 2.5 % to 0.43 GPa at 10 %, while TPG shows a smaller decline from 0.96 GPa to 0.52 GPa. These insights provide a foundation for optimizing functionalized 2D carbon materials for flexible electronics, energy storage, and nanomechanical applications.

CRediT authorship contribution statement

Amirhossein Nikparsa: Methodology, Investigation, Formal analysis. **Reza Ansari:** Supervision, Project administration, Investigation, Conceptualization. **Mohsen Eghbalian:** Writing – original draft, Visualization, Investigation, Formal analysis. **Saeid Sahmani:** Validation, Investigation, Data curation, Conceptualization. **Eligiusz Postek:** Writing – review & editing, Validation, Supervision, Software, Conceptualization.

Declaration of Competing Interest

It is confirmed that there is no conflict of interest, no financial or personal relationships that may be perceived as influencing our work.

Acknowledgment

This research was funded by the Polish National Agency for Academic Exchange (NAWA) under grant No. BNI/ULM/2024/1/00088/U/00001.

Data availability

Data will be made available on request.

References

[1] M.M. Haley, S.C. Brand, J.J. Pak, Carbon networks based on dehydrobenzoannulenes: synthesis of graphdiyne substructures, Angew. Chem. Int. Ed. Engl. 36 (1997) 836–838.
[2] G. Li, Y. Li, H. Liu, Y. Guo, Y. Li, D. Zhu, Architecture of graphditne nanoscale films, Chem. Commun. 46 (2010) 3256–3258.
[3] R.H. Baughman, H. Eckhardt, M. Kertesz, Structure-property predictions for new planar forms of carbon: layered phases containing sp 2 and sp atoms, J. Chem. Phys. 87 (1987) 6687–6699.

[4] M. Shi, X. Sun, Q. Bai, Y. Zhang, S. Yu, M. Liu, L. Wang, W.W. Yu, N. Sui, Graphdiyne/graphene heterostructure supported NiFe layered double hydroxides for oxygen evolution reaction, Colloids Surf. A Physicochem. Eng. Asp. 637 (2022) 128217.
[5] C. Huang, Y. Li, N. Wang, Y. Xue, Z. Zuo, H. Liu, Y. Li, Progress in research into 2D graphdiyne-based materials, Chem. Rev. 118 (2018) 7744–7803.
[6] X. Gao, H. Liu, D. Wang, J. Zhang, Graphdiyne: synthesis, properties, and applications, Chem. Soc. Rev. 48 (2019) 908–936.
[7] Y. Fang, Y. Liu, L. Qi, Y. Xue, Y. Li, 2D graphdiyne: an emerging carbon material, Chem. Soc. Rev. 51 (2022) 2681–2709.
[8] P. Nikparsa, A. Nikparsa, A. Mirzaei, Catalytic behavior of Co/Al2O3 nanocatalyst under external magnetic field, Phys. Chem. Res. 8 (2020) 645–656.
[9] S. Feng, C. Zhao, T. Zhao, Y. Tian, L. Yan, Efficient reduction of nitrobenzene to aniline by metal-free B-doped graphdiyne, Colloids Surf. A Physicochem. Eng. Asp. 655 (2022) 130229.
[10] S.M. Hatam-Lee, A. Rajabpour, S. Volz, Thermal conductivity of graphene polymorphs and compounds: from C3N to graphdiyne lattices, Carbon 161 (2020) 816–826.
[11] B. Mortazavi, F. Shojaei, M. Shahrokhi, M. Azizi, T. Rabczuk, A.V. Shapeev, X. Zhuang, Nanoporous C3N4, C3N5 and C3N6 nanosheets; novel strong semiconductors with low thermal conductivities and appealing optical/electronic properties, Carbon 167 (2020) 40–50.
[12] X. Zheng, S. Chen, J. Li, H. Wu, C. Zhang, D. Zhang, X. Chen, et al., Two-dimensional carbon graphdiyne: advances in fundamental and application research, ACS Nano 17 (2023) 14309–14346.
[13] B. Mortazavi, M. Makaremi, M. Shahrokhi, Z. Fan, T. Rabczuk, N-graphdiyne two-dimensional nanomaterials: semiconductors with low thermal conductivity and high stretchability, Carbon 137 (2018) 57–67.
[14] Y. Li, L. Xu, H. Liu, Y. Li, Graphdiyne and graphyne: from theoretical predictions to practical construction, Chem. Soc. Rev. 43 (2014) 2572–2586.
[15] A. Nikparsa, R. Ansari, M. Eghbalian, Characterization of the mechanical properties of N-triphenylene nanosheet under atomistic defect and thermal gradient by molecular dynamics simulations, Eur. Phys. J. 140 (2025) 84.
[16] R. Matsuoka, R. Toyoda, R. Shiotsuki, N. Fukui, K. Wada, H. Maeda, R. Sakamoto, et al., Expansion of the graphdiyne family: a triphenylene-cored analogue, ACS Appl. Mater. Interfaces 11 (2018) 2730–2733.
[17] Y. Wang, Q. Wu, J. Mao, S. Deng, R. Ma, J. Shi, et al., Lithium and calcium decorated triphenylene-graphdiyne as potential high-capacity hydrogen storage medium: a first-principles prediction, Appl. Surf. Sci. 494 (2019) 763–770.
[18] X. Kan, Y. Ban, C. Wu, Q. Pan, H. Liu, J. Song, Z. Zuo, Z. Li, Y. Zhao, Interfacial synthesis of conjugated two-dimensional N-graphdiyne, ACS Appl. Mater. Interfaces 10 (2018) 53–58.
[19] K. Khan, A.K. Tareen, M. Iqbal, Z. Shi, H. Zhang, Z. Guo, Novel emerging graphdiyne based two dimensional materials: synthesis, properties and renewable energy applications, Nano Today 39 (2021) 101207.
[20] P. Aghdasi, S. Yousefi, R. Ansari, Doping-induced changes in the structural and mechanical properties of germanene monolayers: a DFT-based study, Mater. Sci. Semicond. Process. 174 (2024) 108246.
[21] S. Haghighi, Y. Keramati, M. Eghbalian, R. Ansari, Mechanical properties of defective graphene-reinforced polymer nanocomposite: a molecular dynamics simulation study, Fibers Polym. 26 (2025) 797–812.
[22] B. Mortazavi, M. Shahrokhi, M.E. Madjet, M. Makaremi, S. Ahzi, T. Rabczuk. N-, P-, As-triphenylene-graphdiyne: strong and stable 2D semiconductors with outstanding capacities as anodes for Li-ion batteries, Carbon 141 (2019) 291–303.
[23] M. Salavati, T. Rabczuk, First-principles investigation of N-triphenylene-graphdiyne nanosheets as an anode material for na, K, mg and ca storage, Comput. Mater. Sci. 169 (2019) 109093.
[24] G.M. Psofogiannakis, G.E. Froudakis, Computational prediction of new hydrocarbon materials: the hydrogenated forms of graphdiyne, J. Phys. Chem. C. 116 (2012) 19211–19214.
[25] H. Yu, Y. Xue, Y. Li, Graphdiyne and its assembly architectures: synthesis, functionalization, and applications, Adv. Mater. 31 (2019) 1803101.
[26] P.A.S. Autreto, J.M. De Sousa, D.S. Galvao, Site-dependent hydrogenation on graphdiyne, Carbon 77 (2014) 829–834.
[27] J. Tan, X. He, M. Zhao, First-principles study of hydrogenated graphyne and its family: stable configurations and electronic structures, Diam. Relat. Mater. 29 (2012) 42–47.
[28] S. Rouhi, H. Moradi, Y. Hakimi, F. Nikpour, On the mechanical properties of the graphyne and graphdiyne with patterned hydrogenation and hole: a molecular dynamics investigation, Appl. Phys. A 126 (2020) 465.
[29] A.P. Thompson, H.M. Aktulga, R. Berger, D.S. Bolintineanu, W.M. Brown, P. S. Crozier, P.J. in 't Veld, A. Kohlmeyer, S.G. Moore, T.D. Nguyen, R. Shan, M. J. Stevens, J. Tranchida, C. Trott, S.J. Plimpton, LAMMPS - a flexible simulation tool for particle-based materials modeling at the atomic, meso, and continuum scales, Comput. Phys. Commun. 271 (2022) 10817.
[30] A. Krokhotin, N.V. Dokholyan, Computational methods toward accurate RNA structure prediction using coarse-grained and all-atom models, Methods Enzymol. 553 (2015) 65–89.
[31] J. Polanski. Chemoinformatics. SD Brown, R. Tauler, and BBT-CC Walczak 2009. 459–506..
[32] S. Sahmani, A.M. Fattahi, Development an efficient calibrated nonlocal plate model for nonlinear axial instability of zirconia nanosheets using molecular dynamics simulation, J. Mol. Graph. Model. 75 (2017) 20–31.
[33] S. Sahmani, A.M. Fattahi, Calibration of developed nonlocal anisotropic shear deformable plate model for uniaxial instability of 3D metallic carbon nanosheets using MD simulations, Comput. Methods Appl. Mech. Eng. 322 (2017) 187–207.
[34] M. Eghbalian, M.J. Hashemi, A. Nikparsa, R. Ansari, S. Sahmani, E. Postek, Exploring mechanical properties of net Y: a molecular dynamics examination on the impact of defect density and temperature gradients under uniaxial tension, Comput. Mater. Sci. 258 (2025) 114049.
[35] J. Tersoff, Modeling solid-state chemistry: interatomic potentials for multicomponent systems, Phys. Rev. B 39 (1989) 5566.
[36] J. Tersoff, New empirical approach for the structure and energy of covalent systems, Phys. Rev. B 37 (1988) 6991.
[37] S.L. Mayo, B.D. Olafson, W.A. Goddard, DREIDING: a generic force field for molecular simulations, J. Phys. Chem. 94 (1990) 8897–8909.
[38] Y. Keramati, R. Ansari, S. Haghighi, M. Eghbalian, A molecular dynamics study on mechanical properties of polymer nanocomposites reinforced by two-dimensional nanosheets, Mol. Simul. 50 (2024) 1116–1128.
[39] A. Nikparsa, R. Ansari, M. Eghbalian, Mechanical properties of N-Graphdiyne (C18N6) under tensile stress: a molecular dynamics study, Mol. Simul. 51 (2025) 808–823.
[40] BIOVIA Materials Studio, Dassault Systèmes, San Diego, CA, USA. ⟨https://www.3ds.com/products/biovia/materials-studio⟩ (last visit 11th July 2025).
[41] C. Elias, R.R. Nair, T.M.G. Mohiuddin, S.V. Morozov, P. Blake, et al., Control of graphene's properties by reversible hydrogenation: evidence for graphene, Science 323 (2009) 610–613.
[42] J. Son, S. Lee, S.J. Kim, B.C. Park, H.-K. Lee, S. Kim, J.H. Kim, B.H. Hong, J. Hong, Hydrogenated monolayer graphene with reversible and tunable wide band gap and its field-effect transistor, Nat. Commun. 7 (2016) 13261.
[43] F. Zhao, Y. Raitses, X. Yang, A. Tan, C.G. Tully, High hydrogen coverage on graphene via low temperature plasma with applied magnetic field, Carbon 177 (2021) 244–251.
[44] G.M. Psofogiannakis, G.E. Froudakis, Computational prediction of new hydrocarbon materials: the hydrogenated forms of graphdiyne, J. Phys. Chem. C. 116 (2012) 19211–19214.
[45] Q. Peng, A.K. Dearden, J. Crean, L. Han, S. Liu, X. Wen, S. De, New materials graphyne, graphdiyne, graphone, and graphane: review of properties, synthesis, and application in nanotechnology, Nanotechnol. Sci. Appl. 7 (2014) 1–29.
[46] Y. Gao, W. Yang, B. Xu, Unusual thermal conductivity behavior of serpentine graphene nanoribbons under tensile strain, Carbon 96 (2016) 513–521.
[47] D. Ran, Z. Yuan, N. Wang, P. Zheng, Mechanical behaviour and micro-mechanism of atomically precise edge graphene nanoribbons mechanical cutting guided by hydrogen atom adsorption, Diam. Relat. Mater. 145 (2024) 111106.
[48] Q.X. Pei, Y.W. Zhang, V.B. Shenoy, A molecular dynamics study of the mechanical properties of hydrogen functionalized graphene, Carbon 48 (2010) 898–904.
[49] C. Lee, X. Wei, J.W. Kysar, J. Hone, Measurement of the elastic properties and intrinsic strength of monolayer graphene, Science 321 (2008) 385–388.
[50] ⟨http://www.ks.uiuc.edu/Research/vmd/⟩ (last visit 11th June 2025).
[51] W. Humphrey, A. Dalke, K. Schulten, VMD - visual molecular dynamics, J. Mol. Graph. 14 (1996) 33–38.
[52] A. Stukowski, Visualization and analysis of atomistic simulation data with OVITO–the open visualization tool, Model. Simul. Mater. Sci. Eng. 18 (2010) 015012.
[53] Y. Li, L. Xu, H. Liu, Y. Li, Graphdiyne and graphyne: from theoretical predictions to practical construction, Chem. Soc. Rev. 43 (2014) 2572–2586.
[54] Y. Shao, S. Zhang, M.H. Engelhard, G. Li, G. Shao, Y. Wang, J. Liu, I.A. Aksay, Y. Lin, Nitrogen-doped graphene and its electrochemical applications, J. Mater. Chem. 20 (2010) 7491–7496.
[55] R. Lv, Q. Li, A.R. Botello-Mendez, T. Hayashi, B. Wang, et al., Nitrogen-doped graphene: beyond single substitution and enhanced molecular sensing, Sci. Rep. 2 (2012) 586.